Photonic-Band-Gap Traveling-Wave Gyrotron Amplifier

Photonic-Band-Gap Traveling-Wave Gyrotron Amplifier

E. A. Nanni,[1] S. M. Lewis,[1] M. A. Shapiro,[1] R. G. Griffin,[2] and R. J. Temkin[1]

[1]*Plasma Science and Fusion Center, Massachusetts Institute of Technology, Cambridge, Massachusetts 02139, USA*

[2]*Department of Chemistry and the Francis Bitter Magnet Laboratory, Massachusetts Institute of Technology, Cambridge, Massachusetts 02139, USA*

(Received 10 May 2013; published 6 December 2013)

We report the experimental demonstration of a gyrotron traveling-wave-tube amplifier at 250 GHz that uses a photonic band gap (PBG) interaction circuit. The gyrotron amplifier achieved a peak small signal gain of 38 dB and 45 W output power at 247.7 GHz with an instantaneous −3 dB bandwidth of 0.4 GHz. The amplifier can be tuned for operation from 245–256 GHz. The widest instantaneous −3 dB bandwidth of 4.5 GHz centered at 253.25 GHz was observed with a gain of 24 dB. The PBG circuit provides stability from oscillations by supporting the propagation of transverse electric (TE) modes in a narrow range of frequencies, allowing for the confinement of the operating TE_{03}-like mode while rejecting the excitation of oscillations at nearby frequencies. This experiment achieved the highest frequency of operation for a gyrotron amplifier; at present, there are no other amplifiers in this frequency range that are capable of producing either high gain or high output power. This result represents the highest gain observed above 94 GHz and the highest output power achieved above 140 GHz by any conventional-voltage vacuum electron device based amplifier.

DOI: 10.1103/PhysRevLett.111.235101 PACS numbers: 84.40.Ik, 42.70.Qs, 52.59.Rz

High-power sources in the millimeter wave, submillimeter wave, and THz regime of the electromagnetic spectrum are of great interest due to their potential applications in radar, communications, and spectroscopy [1–9]. Many of these applications require the source to provide phase stability and control. However, amplifiers that can meet this requirement, while providing output power levels of tens to hundreds of watts at frequencies above 140 GHz, are currently not available. Solid-state devices are less attractive for high power generation, especially peak power, due to device heating, scalability, and efficiency issues. Classical microwave tubes, e.g., klystrons and traveling wave tubes, can produce high power electromagnetic radiation up to 100 GHz [10], but these slow wave devices require physical structures in the interaction cavity that are smaller than the wavelength of operation. This small element size produces difficulties with thermal damage and manufacturing of the interaction cavity.

Gyrotrons are a form of electron cyclotron resonance maser. As oscillators they are capable of producing megawatts of output power from microwave to THz bands [6,11–14]. In recent years, gyrotron amplifiers have demonstrated high output power levels with significant gain bandwidths [3,15–22]. A gyrotron amplifier works on the same fundamental principles as a gyrotron oscillator for the extraction of energy from an electron beam. However, the amplifier is operated under conditions that suppress self-start oscillations, including backward-wave oscillations that could disrupt the operation of the device. Amplification is achieved by a convective instability that results from the interaction of a mildly relativistic, annular, gyrating electron beam in a strong static axial magnetic field (B_0) and a transverse electric (TE) waveguide mode. The Doppler shifted electron beam resonance condition is given by

$$\omega - s\Omega/\gamma - k_z v_z = 0 \tag{1}$$

and the waveguide mode dispersion relation is

$$\omega^2 - k_z^2 c^2 - k_\perp^2 c^2 = 0, \tag{2}$$

where ω is the frequency of the wave; $\Omega = eB_0/m_e$ is the nonrelativistic cyclotron frequency; e and m_e are, respectively, the charge and the rest mass of the electron; $\gamma = (1 - v^2/c^2)^{-1/2}$ is the relativistic mass factor; v is the electron velocity; $s = 1$ is the cyclotron harmonic number; k_z and $k_\perp$ are the longitudinal and transverse propagation

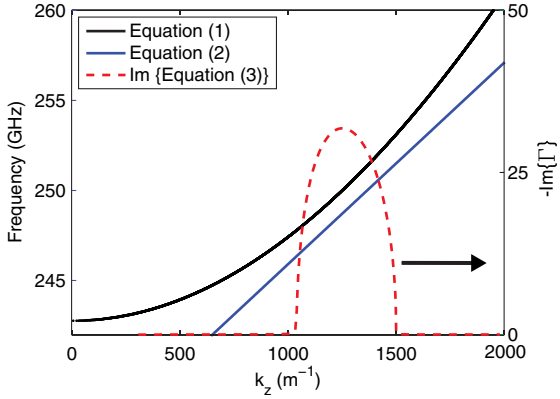

FIG. 1 (color online). Uncoupled and coupled dispersion relations for the waveguide mode and the electron beam for nominal operating conditions. Amplification would be observed when the imaginary part of Γ is nonzero.

constants, respectively, of the waveguide mode; v_z is the axial velocity of the electrons, and c is the speed of light. The uncoupled dispersion relations of the cyclotron resonance mode, (1), and a TE waveguide mode, (2), for a typical operating point are shown in Fig. 1.

The coupled dispersion relation of the amplified wave, which propagates as $e^{ik(\Gamma-\bar{\Delta})z}$, resulting from the interaction between the electron beam and the electromagnetic mode is given by

$$\Gamma^2(\Gamma - \bar{\Delta}) + \bar{\mu} I_0' = 0, \tag{3}$$

where $\beta = v/c$, $k = \omega/c$, $\bar{\Delta} = (1/\beta_{z0}) - (s\Omega/\beta_{z0}\gamma_0\omega) - (k_z/k)$, $\bar{\mu} = (\beta_{\perp 0}^2/2\beta_{z0})(1 - (k_z/k)^2)/(1 - (k_z/k)\beta_{z0})$, k_z is determined from (2), I_0' is the normalized current given in [23], and a small term linear in Γ has been omitted. Equation (3) has three roots corresponding to a growing wave, a damped wave, and an unperturbed wave. The gain of the growing wave for the nominal operating conditions, presented later in this Letter [Fig. 5(b)], is also shown in Fig. 1.

At millimeter or submillimeter wavelengths, operation of a gyrotron amplifier in the lowest order modes, such as the TE_{11} mode or the TE_{01} mode, is unattractive because of the small physical size of the components. For example a TE_{03} mode waveguide with a cutoff frequency of 252.5 GHz has a radius of 1.92 mm and can operate with an electron beam having a 1 mm radius. By comparison, a TE_{01} mode would require a 0.72 mm waveguide radius and a 0.35 mm electron beam radius. Kilowatt power level gyrotron amplifiers have been successfully demonstrated at 140 GHz [17,21] using a novel overmoded (i.e., many modes are above cutoff at the operational frequency) quasioptical interaction structure which consists of a confocal waveguide with severs for additional suppression of oscillations. This mode-selective open waveguide imparts high diffractive losses to the lower order modes which tend to interact with the beam more strongly. This selective loading of the lower order modes allows for stable operation in a higher order mode. Though mode selective, the confocal waveguide has an azimuthally asymmetric field profile which reduces its gain and interaction efficiency with the annular beam produced by the electron gun used in gyrotrons.

Photonic band gap (PBG) structures offer the promise of a frequency selective circuit where the boundary condition at the waveguide "wall" can prevent undesired oscillations. A PBG structure is defined as a periodic structure in one, two or three dimensions that is composed of metal and/or dielectric components where certain frequencies are not allowed to propagate through the lattice. PBG structures have been demonstrated successfully as optical waveguides [24] and accelerator structures [25]. Metallic PBG structures are of interest for gyrotron oscillators [26] and amplifiers to avoid charge buildup on dielectric surfaces. The PBG structure needs to support a TE mode that will not diffract in the transverse direction with respect to the electron beam. The properties of the lattice are governed by the radius, a, and spacing, b, of the rods [27]. These lattice constants are selected to confine a single propagating operational mode, which resides in the lowest band gap, and suppress lower order modes via diffractive losses, which lie outside of any band gap.

A certain number of rods must be removed from the region near the axis to create a defect in which the electron beam and the electromagnetic wave can propagate. This defect region acts as a waveguide where the direction of propagation is along the rod axis. Confinement in the transverse direction is provided by the PBG lattice. The number of rods in the transverse dimension does not need to be infinite, and it can be adjusted to provide the amount of attenuation desired to prevent unwanted oscillations. The TE_{03}-like mode with a cutoff frequency at 242.7 GHz was selected as the operational mode, as shown in Fig. 2(a). Figure 2(b) shows a nearby, poorly confined lower-order mode; note the power diffraction out of the central region. These HFSS [28] simulations with perfectly matched layer boundaries at the external edge provide a diffractive quality factor (Q_{diff}) which is a measure of the mode's confinement. Simulations indicate a loss of -2 dB/cm at 250 GHz with diffractive radiation contributing in -1.7 dB/cm of loss and Ohmic loss contributing -0.3 dB/cm of loss. For the assembled circuit -2.3 dB/cm was measured. To limit Ohmic losses higher conductivity metals could replace the stainless steel rods or a cylindrical waveguide output section could be used in the last few centimeters of the structure where the power is at its highest.

The schematic of the amplifier's primary components is shown in Fig. 3. The electron beam propagates along the axis inside the PBG waveguide. It is generated in a thermionic electron gun. The input power, generated by a VDI, Inc. solid-state source capable of producing 30 mW, enters the circuit at the wraparound coupler [18]. This coupler converts the incident power in the fundamental waveguide into a TE_{03} mode to drive the interaction circuit. The TE_{03}-like mode interacts with the electron beam in the 26 cm PBG circuit. This length was chosen to be just

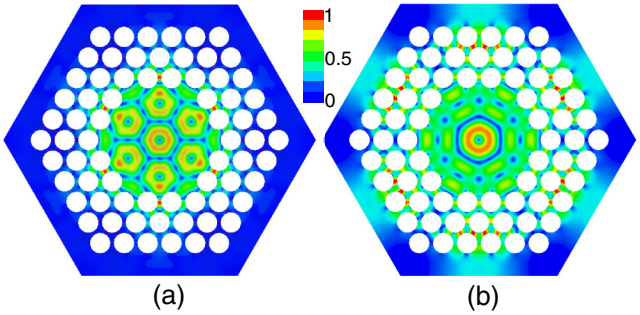

FIG. 2 (color online). Comparison between electric field of PBG waveguide modes with a cutoff frequency of (a) 242.7 GHz and (b) 212.1 GHz. The (a) operational TE_{03}-like mode is well confined ($Q_{\mathrm{diff}} = 1370$) and (b) the lower-order mode is not confined ($Q_{\mathrm{diff}} = 35$). The white circles are stainless steel rods with lattice constants of $a = 0.397$ mm and $a/b = 0.43$.

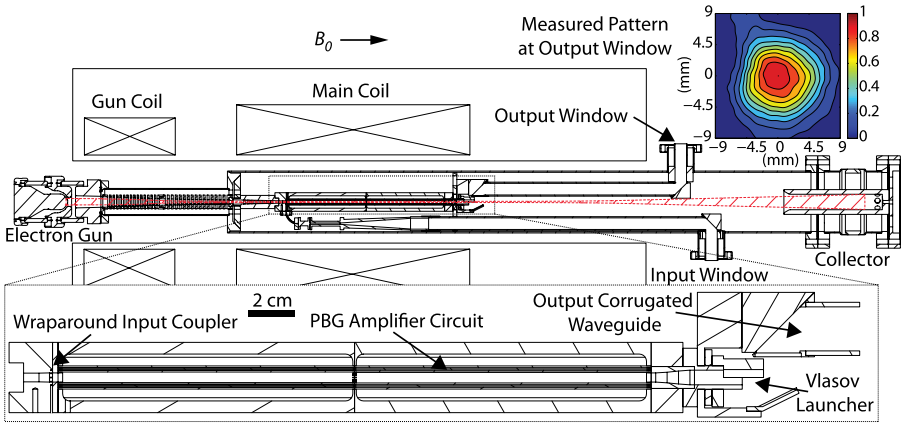

FIG. 3 (color online). Schematic of the PBG amplifier with the electron beam shown with a red dashed line. The measured output pulse radiation pattern is shown at the top right.

smaller than the uniform field length of the magnet, which is 30 cm. Lossy ceramic rings (MACOR) used to support the circuit and to absorb diffracted power from the circuit are not pictured. The interaction is terminated at the uptaper of the Vlasov-type quasioptical launcher [29]. The electron beam exits the circuit and travels to a copper collector. The Vlasov launcher and mirror system transform the TE_{03}-like mode of the PBG circuit into a Gaussian beam which propagates with high efficiency in corrugated waveguides [30]. The Gaussian beam that exits the amplifier will allow for efficient transmission to the intended application [31], a pulsed dynamic nuclear polarization NMR [32] spectrometer. The measured radiated pattern from the amplifier at 247.7 GHz is shown in Fig. 3; it is 92% Gaussian with beam waists of $w_x = 6.6$ mm and $w_y = 6.8$ mm.

A typical amplified pulse measured at the output of the gyrotron is shown in the Fig. 4 insert. The pulse is amplified during the entire 6 μs flat top of the voltage pulse. This pulse was recorded at 245.9 GHz, 31.6 kV, 0.14 A, and 8.77 T. Heterodyne frequency measurements were taken to determine the spectral purity of the amplified pulse, with the frequency spectrum shown on a logarithmic scale in Fig. 4. The amplified gyrotron signal is down-converted from $f_{\mathrm{rf}} = 253.632$ GHz to a Fourier transform peak at $f_{\mathrm{IF}} = 300$ MHz, with the 13th mixer harmonic of $f_{\mathrm{LO,upper}} = 19.487$ GHz. The noise present in the baseline (off) signal, green line Fig. 4, is due to noise from the receiver setup. Noise from the YIG LO which is amplified through the IF channel is the primary contributor to the baseline signal. The measured bandwidth for the 6 μs amplified pulse was 220 kHz in good agreement with the transform limit of this pulse shape.

A theoretical model, based on MAGY [33] a self-consistent time-dependent code that can simulate both gyrotron oscillators and amplifiers, was used for comparison with the measurements taken from the amplifier. The model includes measurements of the input coupler, transmission line, windows, and launcher to incorporate losses. The best coupling into the PBG structure was measured at -12 dB around 247 GHz, but this is located close to the cutoff of the circuit which results in limited bandwidth. For wide bandwidth the amplifier was operated above 252 GHz where the input coupling is approximately flat at -25 dB. It was observed in the experiment that all operating points were limited to a circuit gain of $\sim$50 dB before the onset of operational mode oscillations.

In general, it was observed that the amplifier had two modes of operation: (1) lower in frequency, close to cutoff, yielding modest bandwidth, high gain, and high output power or (2) higher in frequency, far from cutoff, yielding modest gain and wide bandwidths. This behavior of the amplifier is explained by the operating point's proximity to cutoff. As the frequency approaches cutoff, the interaction strength between the electron beam and the electromagnetic wave increases because of the decreased group velocity. However, the rate of change for the group velocity increases limiting the bandwidth.

Figure 5 compares theory and experiment for three different operating points. The velocity spread used in the simulation is very close to the predicted value from

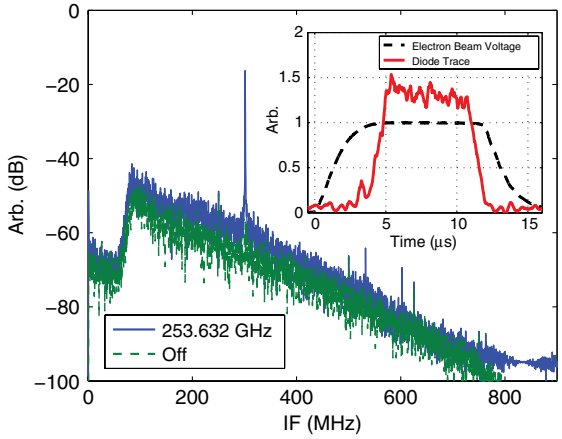

FIG. 4 (color online). Amplified pulse spectrum (blue) down-converted to $f_{\mathrm{IF}} = 300$ MHz. Also shown is the recorded noise spectrum (dashed green) during the voltage pulse when the rf driver is off. Insert: Diode trace measured at the gyrotron amplifier output and the corresponding high voltage pulse.

the electron gun code MICHELLE [34] indicating that the electron gun is performing as expected. The high-gain operating point, which produced 38 dB of gain, 45 W of output power, and a 3 dB bandwidth of 0.4 GHz at 247.7 GHz, is shown in Fig. 5(b). The predicted gain is in good agreement with the measured values; however, the predicted bandwidth does not agree as well. This is believed to be due to additional coupling losses that are not accounted for in the model and may have resulted from misalignments on the input or output transmission line. Figure 5(c) presents an intermediate case for gain and bandwidth, as well as, the lowest operational frequency of the amplifier, which is limited by approaching the waveguide cutoff frequency. The wide-bandwidth operating point with a peak gain of 24 dB, an output power of 4.4 W, and a 4.5 GHz bandwidth at 253 GHz is shown in Fig. 5(d), with good agreement in terms of bandwidth and gain. The input power was measured after an isolator used to protect the solid-state driver and the output power was measured at the output window of the amplifier, Fig. 3, using a Gentec-EO Pyroelectric Joulemeter Probe that is capable of measuring pulse energies exceeding 100 nJ.

One critical aspect for the successful implementation of the amplifier is the constancy of gain with variation of input power. Figure 6 demonstrates that, for two different operating points, as the input signal strength is varied the amplifier gain remains unaffected. The solid and dashed black lines correspond to a linear gain of 35 dB and 25 dB, respectively. When the amplifier was operating with optimized parameters, saturation was not observed due to limited input drive power. Simulations predict a saturated output power on the order of 500 W for the conditions listed in Fig. 5(b).

The development of this gyrotron amplifier is notable for several major advances. At present, there are no other amplifiers in this frequency range that are capable of producing either high gain or high output power. Compared to oscillators, amplifiers offer a much greater challenge requiring matched input and output couplers, excellent beam quality, suppression of mode competition, and interaction over many wavelengths. A more in depth discussion of these differences can be found in review papers, such as Refs. [11–13]. This experiment achieved the highest frequency of operation for a gyrotron amplifier. With 38 dB of gain and 45 W this is the highest gain observed above 94 GHz and the highest output power achieved above 140 GHz by any vacuum electron device; here we exclude free electron lasers powered by accelerators [35,36]. The large bandwidths observed, as much as ~2% of its operational frequency, will allow for the amplification of very short pulses. Previously, pulses as short as 400 ps with pulse broadening and 1 ns without broadening were investigated using a 140 GHz gyrotron amplifier [3]. With the achieved bandwidths reported in this Letter, we would expect that pulses as short as 250 ps could be amplified without broadening. The design of the amplifier is scalable to higher frequencies because the circuit geometry is easy to fabricate and allows for overmoded operation. The amplifier's

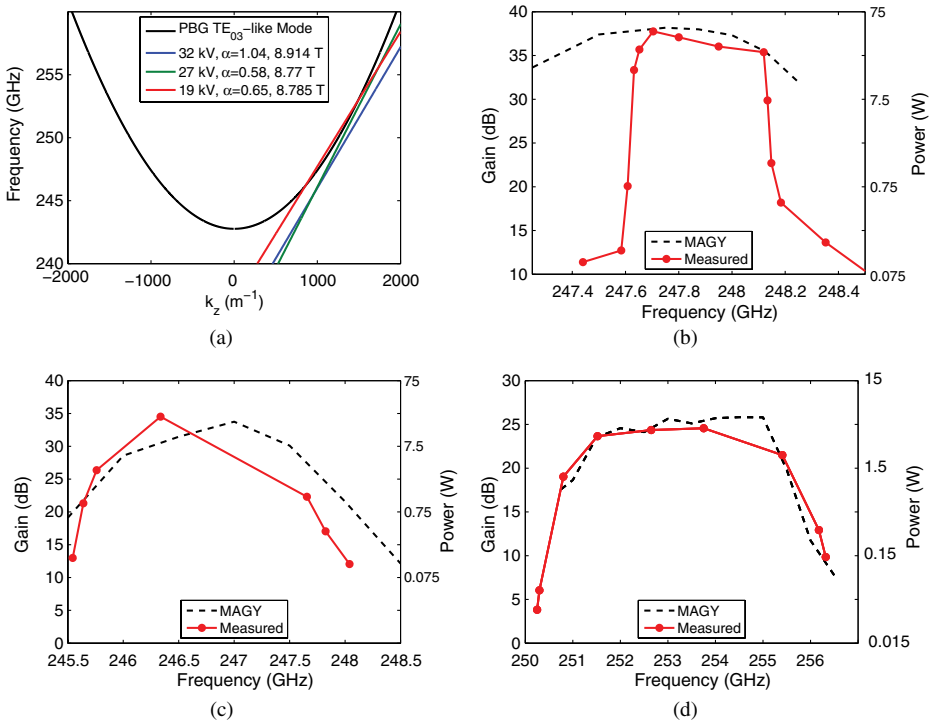

FIG. 5 (color online). (a) Dispersion relations [(1) and (2)] for three operating points with (b) 32 kV, 8.914 T, 0.345 A, 2.5% velocity spread and $P_{in} = 7.5$ mW; (c) 27 kV, 8.77 T, 0.225 A, 4% velocity spread and $P_{in} = 7.5$ mW; (d) 19.3 kV, 8.785 T, 0.4 A, 2% velocity spread and $P_{in} = 15$ mW.

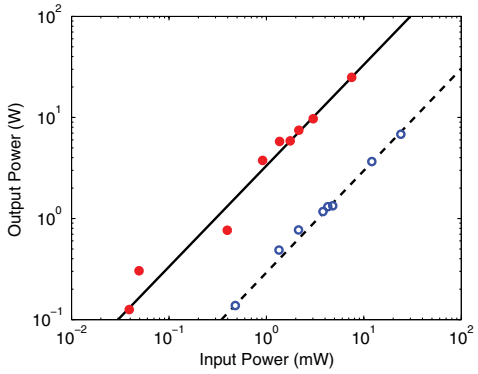

FIG. 6 (color online). Output power vs input power for an input frequency of (red dots) 247.8 GHz at 32.6 kV, 320 mA and 8.9 T; (blue circles) 250.464 GHz at 20.4 kV, 370 mA and 8.83 T.

performance was not limited by the presence of oscillations in lower order modes clearly demonstrating the advantage of a PBG interaction circuit. The output power, output beam pattern, instantaneous bandwidth, spectral purity, and shot-to-shot stability of the amplified pulse meet the basic requirements for the implementation of this device on a pulsed-DNP NMR spectrometer.

The authors gratefully acknowledge Ivan Mastovsky for his assistance. This work was supported by the National Institute of Health (NIH) and the National Institute for Biomedical Imaging and Bioengineering (NIBIB) under Grants No. EB001965 and No. EB004866.

[1] W. He, C. R. Donaldson, L. Zhang, K. Ronald, P. McElhinney, and A. W. Cross, Phys. Rev. Lett. **110**, 165101 (2013).
[2] N. S. Ginzburg, I. V. Zotova, A. S. Sergeev, V. Y. Zaslavsky, and I. V. Zheleznov, Phys. Rev. Lett. **108**, 105101 (2012).
[3] H. J. Kim, E. A. Nanni, M. A. Shapiro, J. R. Sirigiri, P. P. Woskov, and R. J. Temkin, Phys. Rev. Lett. **105**, 135101 (2010).
[4] N. S. Ginzburg, I. V. Zotova, and A. S. Sergeev, Phys. Rev. Lett. **105**, 265001 (2010).
[5] V. L. Bratman, Y. K. Kalynov, and V. N. Manuilov, Phys. Rev. Lett. **102**, 245101 (2009).
[6] M. Y. Glyavin, A. G. Luchinin, and G. Y. Golubiatnikov, Phys. Rev. Lett. **100**, 015101 (2008).
[7] P. H. Siegel, IEEE Trans. Microwave Theory Tech. **50**, 910 (2002).
[8] J. H. Booske, R. J. Dobbs, C. D. Joye, C. L. Kory, G. R. Neil, G.-S. Park, J. Park, and R. J. Temkin, IEEE Trans. Terahz. Sci. Technol. **1**, 54 (2011).
[9] E. A. Nanni, A. B. Barnes, R. G. Griffin, and R. J. Temkin, IEEE Trans. Terahz. Sci. Technol. **1**, 145 (2011).
[10] V. L. Granatstein, R. K. Parker, and C. M. Armstrong, Proc. IEEE **87**, 702 (1999).
[11] K. L. Felch, B. G. Danly, H. R. Jory, K. E. Kreischer, W. Lawson, B. Levush, and R. J. Temkin, Proc. IEEE **87**, 752 (1999).
[12] K. R. Chu, Rev. Mod. Phys. **76**, 489 (2004).
[13] T. Notake, T. Saito, Y. Tatematsu, A. Fujii, S. Ogasawara, L. Agusu, I. Ogawa, T. Idehara, and V. N. Manuilov, Phys. Rev. Lett. **103**, 225002 (2009).
[14] M. K. Thumm, *State of the Art of High Power Gyro Devices and Free Electron Masers* (KIT Scientific Publishing, Karlsruhe, Germany, 2011).
[15] K. R. Chu, H. Y. Chen, C. L. Hung, T. H. Chang, L. R. Barnett, S. H. Chen, and T. T. Yang, Phys. Rev. Lett. **81**, 4760 (1998).
[16] V. L. Bratman, A. W. Cross, G. G. Denisov, W. He, A. D. R. Phelps, K. Ronald, S. V. Samsonov, C. G. Whyte, and A. R. Young, Phys. Rev. Lett. **84**, 2746 (2000).
[17] J. R. Sirigiri, M. A. Shapiro, and R. J. Temkin, Phys. Rev. Lett. **90**, 258302 (2003).
[18] D. E. Pershing, K. T. Nguyen, J. P. Calame, B. G. Danly, B. Levush, F. N. Wood, and M. Garven, IEEE Trans. Plasma Sci. **32**, 947 (2004).
[19] M. Blank, P. Borchard, S. Cauffman, and K. Felch, in *2005 IEEE International Conference on Plasma Science* (IEEE, New York, 2005), p. 112.
[20] M. Blank, P. Borchard, S. Cauffman, and K. Felch, in *2006 International Conference on Infrared Millimeter Waves and Terahertz Electronics* (IEEE, New York, 2006), p. 198.
[21] C. D. Joye, M. A. Shapiro, J. R. Sirigiri, and R. J. Temkin, IEEE Trans. Electron Devices **56**, 818 (2009).
[22] R. Yan, Y. Luo, G. Liu, and Y. Pu, IEEE Trans. Electron Devices **59**, 3612 (2012).
[23] G. S. Nusinovich and H. Li, Int. J. Electron. **72**, 895 (1992).
[24] K. Kuriki, O. Shapira, S. D. Hart, G. Benoit, Y. Kuriki, J. F. Viens, M. Bayindir, J. D. Joannopoulos, and Y. Fink, Opt. Express **12**, 1510 (2004).
[25] E. I. Smirnova, A. S. Kesar, I. Mastovsky, M. A. Shapiro, and R. J. Temkin, Phys. Rev. Lett. **95**, 074801 (2005).
[26] J. R. Sirigiri, K. E. Kreischer, J. Machuzak, I. Mastovsky, M. A. Shapiro, and R. J. Temkin, Phys. Rev. Lett. **86**, 5628 (2001).
[27] E. I. Smirnova, C. Chen, M. A. Shapiro, J. R. Sirigiri, and R. J. Temkin, J. Appl. Phys. **91**, 960 (2002).
[28] HFSS Manual, Ansoft Corp (2012).
[29] S. N. Vlasov and I. M. Orlova, Radiophys. Quantum Electron. **17**, 115 (1974).
[30] E. A. Nanni, S. K. Jawla, M. A. Shapiro, P. P. Woskov, and R. J. Temkin, J. Infrared Millim. Terahz. Waves **33**, 695 (2012).
[31] P. P. Woskov, V. S. Bajaj, M. K. Hornstein, R. J. Temkin, and R. G. Griffin, IEEE Trans. Microwave Theory Tech. **53**, 1863 (2005).
[32] A. Abragam and M. Goldman, Rep. Prog. Phys. **41**, 395 (1978).
[33] M. Botton, T. M. Antonsen, Jr., B. Levush, K. T. Nguyen, and A. N. Vlasov, IEEE Trans. Plasma Sci. **26**, 882 (1998).
[34] J. J. Petillo, E. M. Nelson, J. F. DeFord, N. J. Dionne, and B. Levush, IEEE Trans. Electron Devices **52**, 742 (2005).
[35] S. L. Allen *et al.*, in *Proceedings of the Particle Accelerator Conference, 1993* (IEEE, New York, 1993), pp. 1551–1553.
[36] T. J. Orzechowski, B. R. Anderson, W. M. Fawley, D. Prosnitz, E. T. Scharlemann, S. M. Yarema, A. M. Sessler, D. B. Hopkins, A. C. Paul, and J. S. Wurtele, Nucl. Instrum. Methods Phys. Res., Sect. A **250**, 144 (1986).